doi:10.26443/seismica.v3i2.1420

Foreshocks, aftershocks, and static stress triggering of the 2020 M_w 4.8 Mentone Earthquake in west Texas

David C. Bolton [*1,2], **Nadine Igonin** [3], **Yangkang Chen** [2], **Daniel T. Trugman** [4], **Alexandros Savvaidis** [2], **Peter Hennings** [2]

[1]Institute for Geophysics, Jackson School of Geosciences, University of Texas at Austin, Austin, TX,U.S., [2]Bureau of Economic Geology, Jackson School of Geosciences, University of Texas at Austin, Austin, TX, U.S., [3]University of Texas at Dallas, Department of Sustainability and Earth Systems Sciences, Dallas, TX, U.S., [4]Nevada Seismological Laboratory, University of Nevada at Reno, Reno, NV, U.S

Author contributions: *Conceptualization*: D. Bolton. *Data Curation*: D.Bolton, Y. Chen. *Formal Analysis*: D. Bolton, N. Igonin, D. Trugman. *Funding Acquisition*: P. Hennings. *Investigation*: D. Bolton. *Methodology*: D. Bolton, Y. Chen. *Project Administration*: P. Hennings; A. Savvaidis. *Resources*: Y. Chen, A. Savvaidis. *Software*: D. Bolton, Y. Chen. *Supervision*: D. Trugman, A. Savvaidis. *Validation*: D. Bolton, D. Trugman, N, Igonin. *Visualization*: D. Bolton, D.Trugman. *Writing – original draft*: D. Bolton. *Writing – review & editing*: All authors.

Abstract Foreshocks are the most obvious signature of the earthquake nucleation stage and could, in principle, forewarn of an impending earthquake. However, foreshocks are only sometimes observed, and we have a limited understanding of the physics that controls their occurrence. In this work, we use high-resolution earthquake catalogs and estimates of source properties to understand the spatiotemporal evolution of a sequence of 11 earthquakes that occurred ~ 6.5 hours before the 2020 M_w 4.8 Mentone earthquake in west Texas. Elevated pore-pressure and poroelastic stressing from subsurface fluid injection from oil-gas operations is often invoked to explain seismicity in west Texas and the surrounding region. However, here we show that static stresses induced from the initial M_L 4.0 foreshock significantly perturbed the local shear stress along the fault and could have triggered the Mentone mainshock. The majority (9/11) of the earthquakes leading up to the Mentone mainshock nucleated in areas where the static shear stresses were increased from the initial M_L 4.0 foreshock. The spatiotemporal properties of the 11 earthquakes that preceded the mainshock cannot easily be explained in the context of a preslip or cascade nucleation model. We show that at least 6/11 events are better classified as aftershocks of the initial M_L 4.0. Together, our results suggest that a combination of physical mechanisms contributed to the occurrence of the 11 earthquakes that preceded the mainshock, including static-stressing from earthquake-earthquake interactions, aseismic creep, and stress perturbations induced from fluid injection. Our work highlights the role of earthquake-earthquake triggering in induced earthquake sequences, and suggests that such triggering could help sustain seismic activity following initial stressing perturbations from fluid injection.

Non-technical summary Understanding how earthquakes get started is a fundamental goal of earthquake science. If the early stages of an earthquake can be measured and characterized, then these details could in principle be integrated into models to help advance earthquake early warning systems and earthquake forecasting. Here, we study a sequence of 11 earthquakes leading up to the 2020 Mentone M_w 4.8 mainshock. Seismicity in this area is in large part induced from oil-gas operations, such as wastewater disposal and hydraulic fracturing. The sequence started with a M_L 4.0 earthquake and was followed by a series of 10 smaller M_L 1-2 earthquakes. We show that that the initial M_L 4.0 earthquake increased the stress state along the fault and could have triggered several of the smaller M_L 1-2 earthquakes as well as the mainshock itself. At least 6/11 of earthquakes that followed the initial M_L 4.0 are aftershocks as opposed to foreshocks to the mainshock. Our work demonstrates that the nucleation process of the M_w 4.8 mainshock cannot easily be explained by simple end-member models. Instead, it is likely that a combination of mechanisms contributed to the nucleation and triggering of the 2020 M_w 4.8 Mentone mainshock.

Production Editor: Andrea Llenos
Handling Editor: Ake Fagereng
Copy & Layout Editor: Kirsty Bayliss

Signed reviewer(s): Piero Poli

Received: July 31, 2024
Accepted: December 4, 2024
Published: December 23, 2024

1 Introduction

Earthquake nucleation is broadly defined as the collection of physical processes that lead to unstable frictional slip in the form of an earthquake (Dieterich, 1978, 1986, 1992; Ohnaka, 1992). Because of its inherent connection to the initiation of earthquakes, understanding the nucleation process has important societal implications for advancing earthquake early warning systems, probabilistic seismic hazard analysis, and earthquake forecasting. However, it is still unclear whether the earthquake nucleation process systematically encodes a seismic or geodetic signature that can be accurately detected and characterized in a manner that would foretell catastrophic failure.

Foreshocks, which are small earthquakes that precede and occur near the hypocenter of the impending mainshock, are one type of seismic observation that could lend insights into the earthquake nucleation pro-

*Corresponding author: chas.bolton@beg.utexas.edu

cess (Ohnaka, 1993; Abercrombie et al., 1995; Dodge et al., 1996; Bouchon et al., 2011; Kato et al., 2012; Bouchon et al., 2013; Chen and Shearer, 2013; Brodsky and Lay, 2014; Ruiz et al., 2014; Chen and Shearer, 2015; Kato et al., 2016a,b; Savage et al., 2017; Tape et al., 2018; Trugman and Ross, 2019; Yoon et al., 2019; Kwiatek et al., 2023; Zhu et al., 2022; Moutote et al., 2023; Martínez-Garzón and Poli, 2024; Wang et al., 2024a). Unfortunately, not all earthquakes have foreshocks, which limits their utility in understanding earthquake nucleation processes and the physics that control their occurrence (Jones and Molnar, 1976; Abercrombie and Mori, 1996; Geller, 1997; Wetzler et al., 2022; Peng and Mori, 2022; Zaccagnino et al., 2024). The lack of more routine observations of foreshocks could be connected to an observational bias due to incomplete catalogs (Ross et al., 2019; Brodsky, 2019; Trugman and Ross, 2019) or seismic network resolution. On the other hand, the dearth of foreshock activity prior to crustal earthquakes could be an intrinsic property of how earthquakes start and could reflect the stochastic nature of the nucleation phase. In any case, scientific progress in this domain requires these details to be identified, characterized, and integrated into physics-based models of nucleation (Ellsworth and Beroza, 1995; Mignan, 2014; Gomberg, 2018; McLaskey, 2019).

Foreshocks are often explained in the context of a preslip model, cascade model, or a combination of both (Ellsworth and Beroza, 1995; Beroza and Ellsworth, 1996; McLaskey, 2019; Cattania and Segall, 2021; Martínez-Garzón and Poli, 2024). In the preslip model, foreshocks are thought to be a byproduct of an aseismic creep front that loads frictionally locked asperities along the fault zone (Ellsworth and Beroza, 1995). This model is consistent with laboratory observations showing that dynamic instability is often preceded by an accelerating zone of aseismic creep (Scholz et al., 1972; Dieterich, 1978, 1986, 1992; Ohnaka and Shen, 1999; McLaskey, 2019). The laboratory data and theoretical models further show that this accelerating zone of aseismic creep must reach a critical nucleation length, often termed h^*, before seismic slip can proceed (Dieterich, 1978, 1986; Ohnaka and Shen, 1999; McLaskey, 2019). In laboratory experiments and numerical models, the critical nucleation length scale, h^*, can be calculated as:

$$h^* = \frac{G * Dc}{(b-a) * (\sigma_N - P_p)}) \quad (1)$$

Where G is the shear modulus, D_c is the frictional weakening distance, *(b-a)* is the frictional-rate parameter, σ_N is the normal stress, P_p is the pore-fluid pressure, and (σ_N-P_p) is the effective normal stress. In the preslip model foreshocks are viewed as being an intrinsic part of the nucleation process of the impending mainshock and their spatiotemporal properties could provide insights into this process. In contrast, the cascade-model views foreshocks as part of a stochastic process that are simply a manifestation of earthquake-earthquake triggering from static stress transfer (Ellsworth and Beroza, 1995; Helmstetter and Sornette, 2003; Ellsworth and Bulut, 2018; Yoon et al., 2019). In the cascade model, each foreshock triggers the next foreshock and eventually triggers the mainshock. In this case, foreshocks are not deterministically linked to the impending mainshock. In the cascade model, small and large earthquakes initiate in a similar manner; the only difference between a small foreshock and a large mainshock is that the larger mainshock encountered favorable fault conditions (e.g., stress, strength, frictional properties) that permitted a larger area to rupture. It's important to note that the cascade and preslip models are simplified endmembers. Hybrid models that integrate aspects of both the preslip and cascade models might be better alternatives for explaining the complexities associated with foreshock sequences (McLaskey, 2019; Cattania and Segall, 2021).

The preslip and cascade models have been widely used to explain foreshocks and nucleation processes prior to regular tectonic earthquakes (Ellsworth and Bulut, 2018; Yoon et al., 2019; Martínez-Garzón and Poli, 2024; Wang et al., 2024a). However, it is unclear whether these models can be extended to explain induced earthquake sequences, where the role of pore-pressure and poroelastic stressing likely play an important role in earthquake nucleation (see also Wu and McLaskey, 2022). The critical nucleation length, h^*, scales directly with pore-pressure (see Equation 1). Hence, elevated fluid pressure from waste-water injection should facilitate larger amounts of creep prior to instability and should push the fault towards stability (e.g., Leeman et al., 2016; Pepin et al., 2022). If foreshocks are a manifestation of fault creep, as proposed in the preslip model, then one might expect elevated foreshock occurrence prior to fluid-induced earthquakes simply because the nucleation dimension is larger relative to the case when pore-pressure is quasi-static (e.g. Cebry et al., 2022). Indeed, two of the largest induced earthquakes in Oklahoma, including the 2011 M_w 5.7 Prague Oklahoma earthquake and the 2016 M_w 5.8 Pawnee earthquake, were preceded by foreshock sequences (Sumy et al., 2014; Savage et al., 2017; Chen et al., 2017). Detailed analysis and modeling indicate that both aseismic creep and elastic stress transfer likely played a key role in triggering the foreshocks.

Alternatively, elevated fluid pressure could initiate fluid-driven aseismic creep along rate-strengthening fault patches, which in turn, load frictionally unstable patches to generate foreshocks (e.g., Guglielmi et al., 2015; Cappa et al., 2019; Cebry and McLaskey, 2021; Cebry et al., 2022). In this case, the fluid-induced aseismic creep need not be a part of an intrinsic nucleation phase of the mainshock and could be a manifestation of frictional heterogeneity in conjunction with a small nucleation length scale (e.g., Cascade model; McLaskey, 2019). In addition, elevated fluid pressure from subsurface fluid injection may trigger foreshocks by increasing elastic stresses on the fault through poroelastic effects (e.g., Segall and Lu, 2015; Goebel et al., 2017; Goebel and Brodsky, 2018). Hence, fluid pressure may affect earthquake nucleation and foreshock occurrence in ways that extend beyond the basic concepts encapsulated in the preslip and cascade models.

In this work, we investigate the causative factors be-

hind 11 earthquakes that preceded the 2020 M_w 4.8 Mentone earthquake, as well as the mainshock itself. The bulk of the seismicity in west Texas is induced from stress perturbations associated with subsurface fluid-injection from oil-gas operations (Tung et al., 2021; Zhai et al., 2021; Jin et al., 2023; Tan and Lui, 2023; Smye et al., 2024). However, the role of earthquake-earthquake triggering in west Texas, and induced earthquake sequences more broadly, has received little attention. Here, we test whether earthquake-earthquake triggering can explain the 11 events that preceded the mainshock and the nucleation of the Mentone mainshock. We test the efficacy of the cascade model by modeling the static shear stresses induced from previous earthquakes (e.g., Ellsworth and Bulut, 2018; Yoon et al., 2019). Our work shows that the Mentone mainshock nucleated in an area where the shear stress could have increased between 60-400 kPa from the initial M_L 4.0 foreshock, far greater than previously modeled Coulomb stresses from fluid injection (e.g., Tung et al., 2021; Tan and Lui, 2023; Smye et al., 2024). The majority of the earthquakes that preceded the mainshock nucleated in areas where the stresses were increased from the M_L 4.0 and several earthquakes have overlapping source radii. We conclude that neither the preslip nor cascade model can successfully explain the occurrence of all 11 earthquakes that preceded the Mentone mainshock. At least 6/11 earthquakes are better classified as aftershocks of the initial M_L 4.0 foreshock.

1.1 The 2020 M_w 4.8 Mentone Earthquake

On March 26, 2020, a M_w 4.8 earthquake struck (from here forward referred to as the mainshock) ~ 175 km west of Odessa, Texas (Figure 1A Skoumal et al., 2020; Tung et al., 2021; Tan and Lui, 2023). The mainshock occurred at a depth of ~ 6 km and resulted from slip along a normal fault, striking ~ 64° and dipping 65° to the southeast (Horne et al., 2021; Huang et al., 2022). The fault geometry is estimated from fault mapping, earthquake data, and focal plane solutions from Horne et al. (2021). The mainshock occurred within the Delaware Basin, a prolific oil and gas producing basin located within the larger Permian Basin of west Texas and southern New Mexico, which has experienced a rapid uptick in seismicity since ~ 2016 (Skoumal and Trugman, 2021). The seismicity in this region is associated with subsurface disposal of wastewater into shallow (< 3 km) and deep formations (> 3 km) and, to a lesser extent, hydraulic fracturing (Savvaidis et al., 2020; Grigoratos et al., 2022). Previous work has indicated that the injection of large volumes of waste-water injection into deep formations could have potentially triggered the 2020 Mentone mainshock by reducing the effective normal stress on the fault via pore-pressure diffusion (Tung et al., 2021; Smye et al., 2024). Modeling results show that pore-pressure and poroelastic stressing from fluid injection into deep strata (~ 5 km) increased the Coulomb failure stress by ~ 80 kPa at the location of the Mentone earthquake. In addition, Tan and Lui (2023) show that waste-water injection into shallow strata (< 2 km) could have imparted ~ 20 kPa of stress at the mainshock hypocenter through far-field poroelastic stresses. However, these studies ignore the role of static triggering from nearby seismicity and its potential role in triggering or leading to a clock-advance of the Mentone mainshock.

1.2 Definition of foreshocks and their spatiotemporal patterns

Foreshocks are small earthquakes that precede and occur near the hypocenter of the impending mainshock. Because foreshocks can only be identified in hindsight after a larger earthquake has occurred, there is not always an obvious space-time window that robustly defines foreshocks. Previous investigators have defined foreshocks using window sizes that vary from hours to months and spatial windows <= 30 km (Chen and Shearer, 2013; Ellsworth and Bulut, 2018; Yoon et al., 2019; Peng and Mori, 2022; Wetzler et al., 2022; Jones and Molnar, 1976). If earthquakes start in a manner that is consistent with theoretical models, then the critical nucleation length scale (h^*) could qualitatively constrain the expected size of the foreshock region (McLaskey, 2019; Wu and McLaskey, 2022).

We start our analysis by enhancing the TexNet catalog using a machine learning phase-picker, EQCCT, and relocate the events with GrowClust (Saad et al., 2023; Trugman and Shearer, 2017, Figure 1). We identified 45 earthquakes leading up to the Mentone mainshock within a 3-month time window and a 5 x 5 km^2 area surrounding the hypocenter (Figures 1A-C). Our choice of window size is strictly empirical and is based upon the spatiotemporal characteristics of the foreshocks relative to the mainshock. Indeed, there are several M_L 2+ earthquakes that occurred within the months leading up to the mainshock. However, we ignored these events in our analysis because they do not exhibit spatiotemporal patterns that would lend confidence in the idea that they are indeed foreshocks, and a part of the nucleation process of the M_L 4.9 mainshock (e.g., Dodge et al., 1996; Kato et al., 2016a,b; Yoon et al., 2019). Earthquakes with failure times > 6.5 hours from the mainshock do not show spatial migration along the fault that would be indicative of an expanding nucleation zone as described in the preslip model (e.g., Dodge et al., 1996; Kato et al., 2016a,b). In addition, these events do not show a systematic migration towards the mainshock as documented in previous foreshock sequences (e.g., Dodge et al., 1996; Yoon et al., 2019). Finally, their large time lag with respect to the mainshock makes it difficult to explain their occurrence under a cascade model, where static triggering should occur over relatively short time scales (Ellsworth and Bulut, 2018; Yoon et al., 2019).

Interestingly, a sequence of 11 earthquakes occurred ~ 6.5 hours before the mainshock (Figures 1B,1D, 2A). We refrain from calling all these events as foreshocks because as we will show below its possible that a majority (6/11) are better characterized as aftershocks of the M_L 4.0. This collection of 11 earthquakes produced a notable uptick in the seismicity rate as is often observed in laboratory experiments (e.g., Dresen et al.,

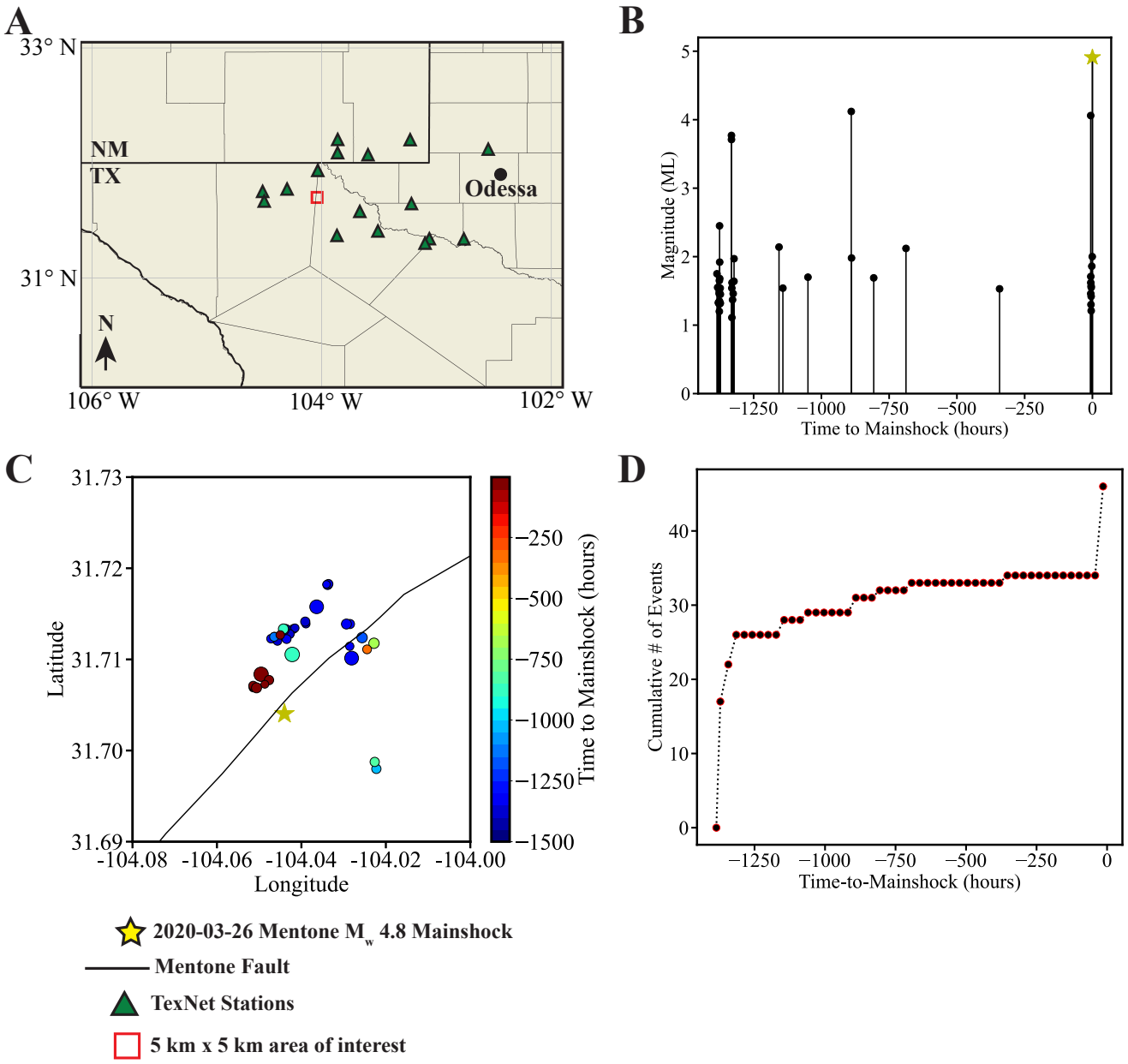

Figure 1 A: Map view of west Texas and southeastern New Mexico. Red box highlights the 5 x 5 km^2 study area. B: Temporal evolution of seismicity in the 3-months before the Mentone mainshock. C: Map view of the earthquakes plotted in panel B. D: Cumulative number of earthquakes leading up to the Mentone mainshock. The increase in event rates immediately before the mainshock is due to the 11 earthquakes that nucleated ~ 6.5 hours before the mainshock (see Figure 2).

2020; Trugman et al., 2020; Bolton et al., 2021), and prior to some large crustal earthquakes (Kato et al., 2016a,b; Yoon et al., 2019). The sequence that occurred in the 6.5 hours before the mainshock started with a M_L 4.0 and was followed by ten events with magnitudes between M_L 1-2. When plotted in map view, 8/11 events are located within a small ~ 500 x 500 m^2 area (Figures 2B-D). For clarity, we refer to these events as the "main-cluster". The remaining three events are considered outliers in the sense that they are disconnected in space from the main cluster of events (Figures 2B,2D). Note, that the relative event locations returned from GrowClust are highly constrained, with average horizontal and depth uncertainties of ~ 30 m and 130 m, respectively. Uncertainties returned from GrowClust correspond to the median absolute deviations in source locations and are estimated using a bootstrapping technique (see Trugman and Shearer, 2017). Due to uncertainties in fault mapping and the velocity model used in GrowClust, the earthquakes do not align perfectly along the projected fault trace. However, this misalignment does not influence the results presented here which are more sensitive to the relative location uncertainties (i.e., distance between events), and are highly constrained from GrowClust, rather than the absolute positions of events. We project the 11 earthquakes and mainshock onto the fault plane in Figure 2B (along the A-A' trace) and plot their locations along strike as a function of time to the mainshock and depth in Figures 2C-D. The along strike distance is referenced to (-104.070°, 31.693°) and extends to (-104.030°, 31.700°). The earthquakes do not show a systematic migration along the fault plane leading up

to the mainshock, as is observed in some foreshock sequences (Figures 2B-D; Dodge et al., 1996; Ellsworth and Bulut, 2018; Kato et al., 2016a; Yoon et al., 2019).

2 Assessing the role of static stress triggering on earthquake occurrence

We start our analysis by testing the hypothesis that the 11 events that preceded the Mentone mainshock are indeed foreshocks of the Mentone earthquake. We then test the validity of the cascade model and whether earthquake-earthquake triggering can explain the occurrence of the 11 earthquakes that preceded the mainshock.

The rupture radius and average slip of each earthquake is needed to model the slip and shear stress perturbation imparted by each event and to test the efficacy of the cascade model (e.g., Dodge et al., 1996; Ellsworth and Bulut, 2018; Yoon et al., 2019). The rupture radius can in theory be estimated from the corner frequency of the source spectrum (see Equation S1 in Supplement). In practice, corner frequencies are challenging to measure using noisy and bandlimited seismic data (Abercrombie, 2021). For example, estimating corner frequencies and source properties for small earthquakes (M < 3) is particularly challenging because to do so requires adequate signal-to-noise at high frequencies (> 10 Hz), which is often outside the resolvable bandwidth of seismic data (Figure S4). Here, we employ Empirical Greens Functions (EGF) to estimate the corner frequency and source radius of the initial M_L 4.0 foreshock (see supplement for details). We attempted to measure the corner frequencies of the smaller foreshocks (M_L 1-2) using EGFs, but this proved unsuccessful due to the bandlimited nature of the seismic data (Figure S5). Therefore, we assume that the smaller M_L 1-2 earthquakes are representative of the 3000+ earthquakes analyzed in the Delaware Basin by Trugman and Savvaidis (2021) and assume that they have stress drops between 0.5-8 MPa. We use a 2 MPa stress drop as our baseline, which is median stress drop found by Trugman and Savvaidis (2021), and perform a sensitivity analysis on our results using a 0.5 and 8 MPa stress drop, respectively (see Supplement). This represents a $\pm$4x range around our baseline of 2 MPa and accounts for the expected event-event variations in stress drops in the Delaware Basin (Trugman and Savvaidis, 2021). We show below that our results are independent of the choice of stress drop for the small M_L 1-2 earthquakes. Following the work of Eshelby (1957), we can then measure the rupture radius of each earthquake as:

$$a = \left(\frac{7M_o}{16\Delta\sigma} \right)^{\frac{1}{3}} \tag{2}$$

To gain insights into the connections between earthquakes, we plot the rupture area for each foreshock and mainshock (Figure 3). Note, that this analysis is strongly contingent upon the relative location uncertainties, which are indeed highly constrained from GrowClust (i.e., uncertainties <130 m). Earthquakes with a time-to-failure (TTF) of 383, 369, 362, 360, 319, 271, and 38 (min) are co-located to within one rupture radius from each other and some events re-rupture a portion of the fault that slipped during the first foreshock or in subsequent foreshocks (Figure 3B). In particular, events with a TTF of 369, 360, 319, and 38 (min) have overlapping source radii, and appear to be indicative of repeating earthquakes (Uchida and Bürgmann, 2019). To confirm the possibility that these events are repeaters, we cross-correlate their waveforms using a 10.5-s window surrounding the S-wave data (Figure 3C). The data show that events with a TTF of 369, 360, 319, 38 (min) have cross-correlation coefficients > 0.7 and can be considered as repeaters (Figures 3B-C). Also note that the observations in Figure 3 remain valid for stress drops between 0.5-8 MPa for the small M_L 1-2 foreshocks (Figure S6).

Finally, assuming circular ruptures and using measurements of the source radius, a, and seismic moment, we can then measure the average slip across the fault plane, u, using the following:

$$u = \frac{M_o}{G * \pi * a^2} \tag{3}$$

Here G represents the shear modulus, which we set as 30 GPa to be representative of the basement rocks, and a represents the source radius from Equation 2. For the M_L 4.0 foreshock we use an EGF approach to estimate the corner frequency and apply equation S5 to estimate the source radius (see Supplement). We follow previous investigators and model the resulting slip and shear stress distribution within and surrounding the circular fault patch using the model presented in Andrews (1980) (Ellsworth and Bulut, 2018; Yoon et al., 2019; Wang et al., 2024a). In this model, the slip varies as a function of position with the circular fault patch and is azimuthally symmetric; fault slip is highest at the center of the circular fault patch and tappers off gradually to zero at the edges (Figure S7A,C). The slip distribution is modeled as:

$$d(r) = \begin{cases} u\left[1 - \frac{r}{a}^2\right]^{\frac{3}{2}} & r < a \\ 0 & r > a \end{cases} \tag{4}$$

where r is the radius within the fault plane, a is the earthquake source radius from Equation 2, u is the average slip in Equation 3. Shear stresses are estimated in the Fourier domain by multiplying the slip by a stiffness function derived in Andrews (1980). In this model, the resulting slip from the earthquake reduces the shear stress within the fault patch and increases the shear stress at the edges which then decreases rapidly with distance from the rupture tip (Figure S7 B,D). We use this model because it has been routinely used in previous works to study foreshock interactions prior to the 1999 M_w 7.1 Hector Mine, 1999 M_w 7.6 Izmit, and 2021 M_w 6.1 Yangbi earthquakes (Ellsworth and Bulut, 2018; Yoon et al., 2019; Wang et al., 2024a). Here we use the modeling results to test whether the 11 earthquakes that preceded the Mentone mainshock observed in Figure 1 can be explained by static stress transfer from earthquake-earthquake triggering as described in the cascade model (Ellsworth and Beroza, 1995).

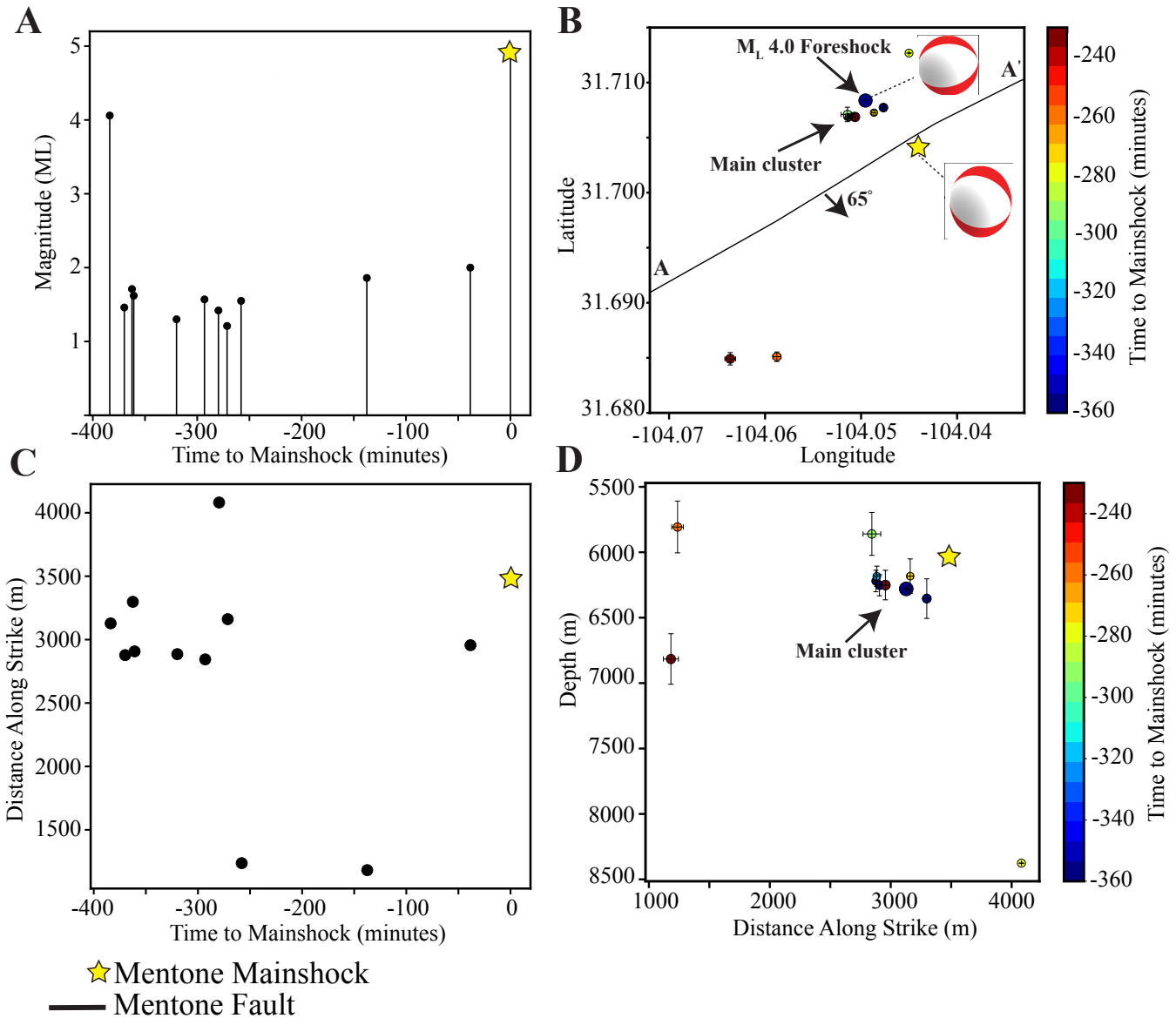

Figure 2 A: Stem plot showing the sequence of 11 earthquakes in the final ~ 6.5 hours leading up to the Mentone mainshock. The sequence started with a M_L 4.0 foreshock and was followed by 10 smaller earthquakes with M_L 1 − 2. B: Map view of seismicity from panel A. Earthquakes are denoted with circles and color-coded according to the origin time of the mainshock. Location uncertainties are derived from a bootstrapping technique described in Trugman and Shearer (2017). Also, plotted are focal mechanisms from TexNet and the fault trace associated with the Mentone earthquake from Horne et al. (2021); fault dip direction and angle are depicted with arrow. Note, that most of the earthquakes (8/11) occur in a localized region near the mainshock. For clarity purposes, we label this set of events as the "main-cluster". C: Earthquake locations along strike after projecting them onto the fault trace shown in panel B from A-A'. Distance along the fault strike starts at a longitude of -104.070 and extends to -104.030. Earthquakes do not show systematic progress along the strike of the fault as a function of time to the mainshock. D: Depth cross-section view of earthquake locations after projecting locations onto the fault plane. Similar to panel B, earthquakes show a strong spatial clustering as a function of depth. Note, that the three events that lie outside of the main cluster are disconnected along the strike of the fault as well as in depth.

We assume that the sequence of 11 earthquakes and mainshock are co-planar (Figure 2B). The fact that the focal mechanisms of the mainshock and the largest M_L 4.0 foreshock are consistent with one another, and the average uncertainties of the relative locations returned from GrowClust are < 130 m lends confidence in this assumption (Figure 2). Note that the models do not consider a particular slip direction. In each subpanel of Figure 4, we label the earthquake associated with the current TTF as the "current" earthquake and the subsequent earthquake as the "impending". In addition, each subpanel is color-coded by the cumulative static shear stress imparted by the previous events; areas marked in red show locations along the fault where the shear stress has increased while areas in blue denote areas where the shear stress has decreased. Assuming a 2 MPa stress drop for the small M_L 1-2 earthquakes, the data in Figure 4 show that the majority (9/11) of the events labeled as "current" earthquakes nucleated in areas where the shear stress was increased from pre-

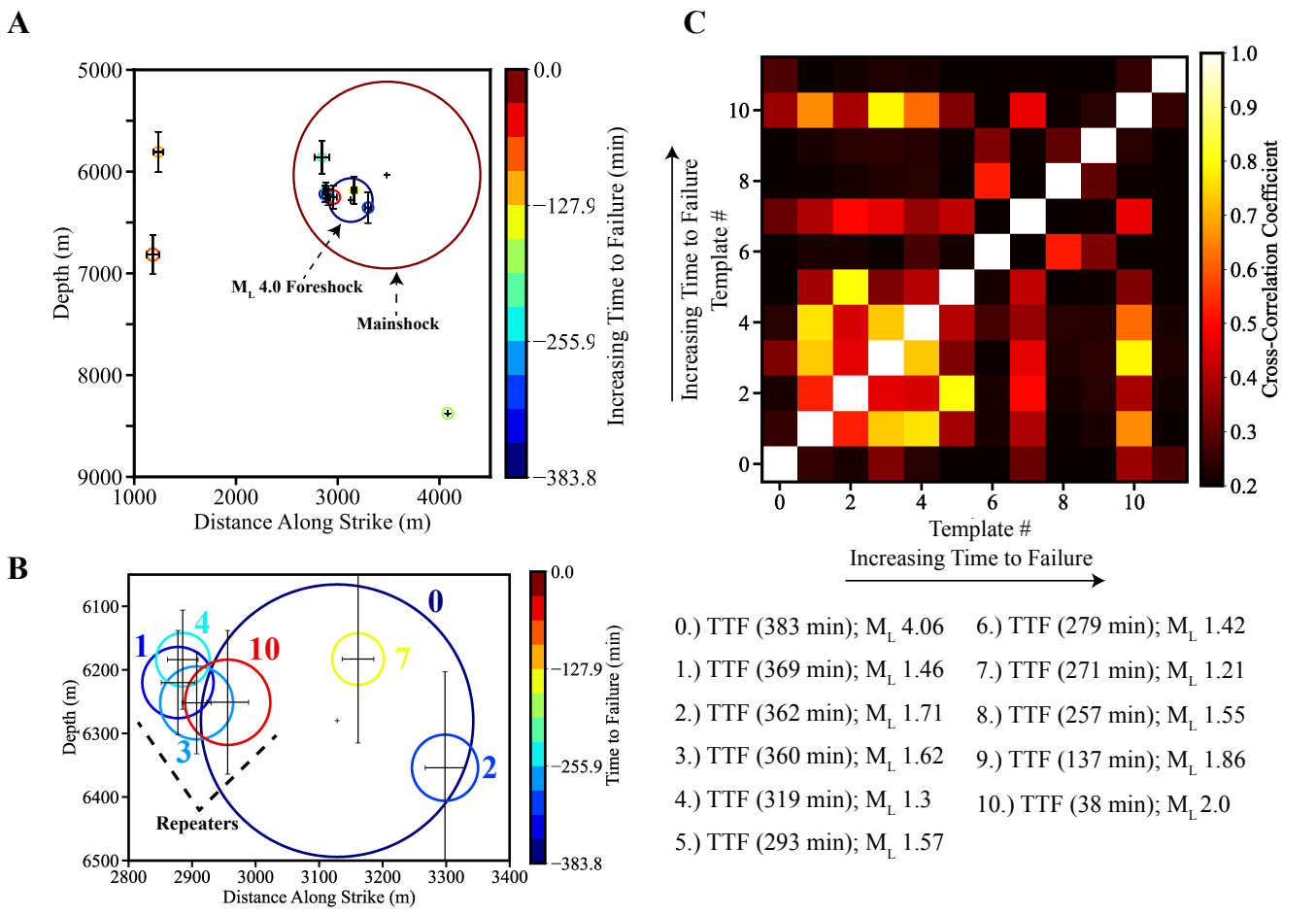

Figure 3 A: Source radii of mainshock and sequence of 11 earthquakes that preceded the mainshock plotted along the fault plane. Source radii for M_L $1-2$ earthquakes and mainshock are derived assuming a constant stress drop of 2 MPa. Rupture radius of the M_L 4.0 foreshock is calculated using EGFs. Circles are color coded according to time until the mainshock, which we denote as time-to-failure (TTF). Error bars represent relative location uncertainties from GrowClust. B: Zoom of "main cluster" of events in A. The data show that ~ 7/11 earthquakes re-ruptured areas along the fault plane that slipped in previous events. Note events are labeled according to their template number (see figure legend) C: Cross-correlation matrix of the 11 earthquakes that preceded the mainshock. Template numbers 1,3,4, and 10 all have high waveform similarity (> 0.70) and overlapping source radii.

vious events, particularly the initial M_L 4.0. The "current" earthquake in panel 4H is the only event that nucleated in an area where the shear stress decreased (see also Figure 5B); however, considering the depth uncertainty of this event it is possible that this event was also located in an area where the shear stress was increased from the M_L 4.0. The initial M_L 4.0 foreshock imparted most of the shear stress at the location of the Mentone mainshock, while the remaining 10 events imparted < 2 kPa of shear stress at the mainshock hypocenter (Figures 5A-B). When accounting for uncertainties in event locations the static stresses induced at the Mentone mainshock from the initial M_L 4.0 foreshock range from ~ 60-400 kPa (Figure 5C). Events with TTF of 137.5, 257, and 279 (min) nucleated in areas where the shear stress increased between 1-2 kPa. Note, these events lie outside of the "main-cluster" identified in Figure 2D. The spatiotemporal evolution of the events and the associated static-stresses do not evolve systematically through a series of cascading ruptures as is observed in some foreshock sequences (e.g., Yoon et al., 2019; Ellsworth and Bulut, 2018). We demonstrate that the results highlighted in Figures 3-5 are valid for stress drops between 0.5-8 MPa for the small M_L 1-2 earthquakes (Figures S8-11). This indicates that the static-shear stresses induced along the fault plane were largely controlled by the initial M_L 4.0 foreshock as opposed to the smaller M_L 1-2 earthquakes.

3 Discussion

Distinguishing between the cascade and preslip model is challenging and has led to different interpretations of the same foreshock sequence. For example, both mechanisms have been invoked to explain the foreshocks preceding the 1999 M_w 7.1 Hector Mine (Chen and Shearer, 2013; Yoon et al., 2019), 1999 M_w 7.6 Izmit (Bouchon et al., 2011; Ellsworth and Bulut, 2018), and the 2021 M_w 6.4 Yangbi mainshocks (Zhu et al., 2022; Zhou et al., 2022). In general, the cascade model pre-

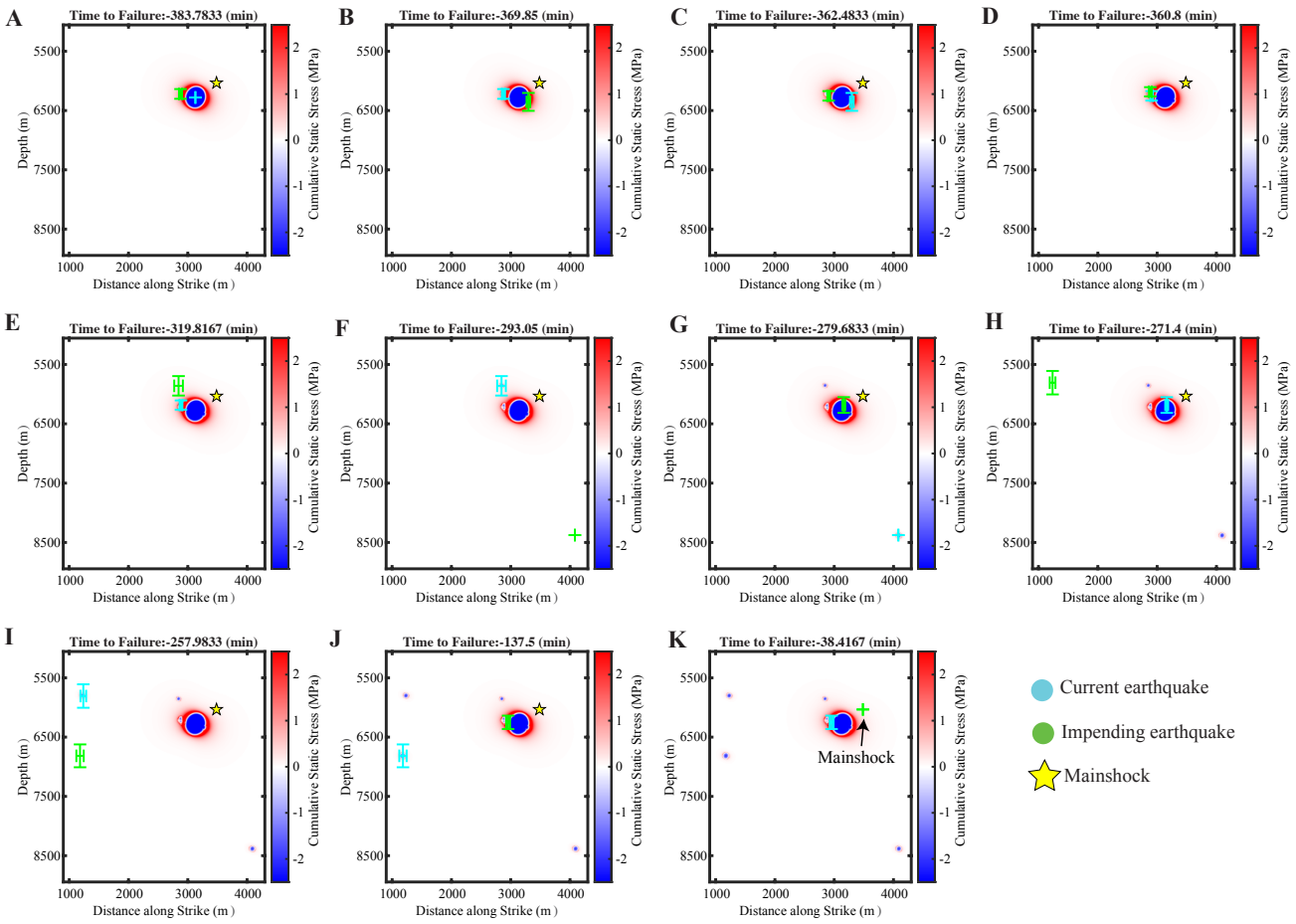

Figure 4 The Mentone sequence plotted along the fault plane as a function of time to the main-shock origin time (denoted here as time-to-failure). In each subplot, we plot the location of the "current" earthquake with a cyan circle and the impending earthquake with a green circle. The fault plane is color coded by the cumulative static stress imparted from previous earthquakes. Static stresses are computed assuming a 2 MPa stress drop for the M_L 1−2 earthquakes. Note, that the static-stresses along the fault plane are dominated from the stress perturbation imparted by the first foreshock (M_L 4.0). 9/11 earthquakes nucleated in areas that experienced an increase in shear stress from the initial M_L 4.0 foreshock. Only one event (i.e., the "current" earthquake in panel H) nucleated in area where the shear stress decreased from previous earthquakes.

dicts that foreshocks should nucleate in areas along the fault plane that have experienced an increase in shear stress from previous foreshocks. In addition, rupture areas between neighboring foreshocks should abut with little overlap (Ellsworth and Bulut, 2018; Yoon et al., 2019). In the preslip model, foreshocks are a byproduct of accelerated aseismic creep that occurs within the nucleation zone of the impending mainshock (Mignan, 2014; Gomberg, 2018; McLaskey, 2019). Key features of the preslip model include accelerated seismicity in space and time preceding the mainshock, independent geodetic observations of aseismic creep, repeating earthquakes, and spatial growth in foreshock activity along the fault (Ohnaka, 1992, 1993; Dodge et al., 1996; Bouchon et al., 2011; Kato et al., 2016a,b; McLaskey, 2019). A common feature of some foreshock sequences is their tendency to migrate towards the hypocenter of the mainshock which can occur in both models (Dodge et al., 1996; Kato et al., 2016a,b; Ellsworth and Bulut, 2018; Yoon et al., 2019). Distinguishing between these two mechanisms can only be discriminated in special cases where there are precise earthquake locations, high-quality source properties, and details of rupture propagation. Obtaining such high-quality measurements for small earthquakes (M_L < 3), such as those in induced earthquake sequences, is particularly challenging due to sparse observations and band-limited seismic data. Furthermore, aftershock sequences that follow large foreshocks add additional complexities that make it challenging to understand the precise connection between foreshocks and the nucleation process of the impending mainshock.

Despite these challenges, our work reinforces the idea that invoking a single mechanism to describe foreshock sequences, such as those described in the preslip model and cascade model, is likely insufficient in explaining all foreshocks and additional mechanisms need to be accounted for (McLaskey, 2019; Martínez-Garzón and Poli, 2024). Furthermore, our work highlights the importance of earthquake-earthquake triggering in induced earthquake sequences and suggests that it could help sustain seismic activity following the

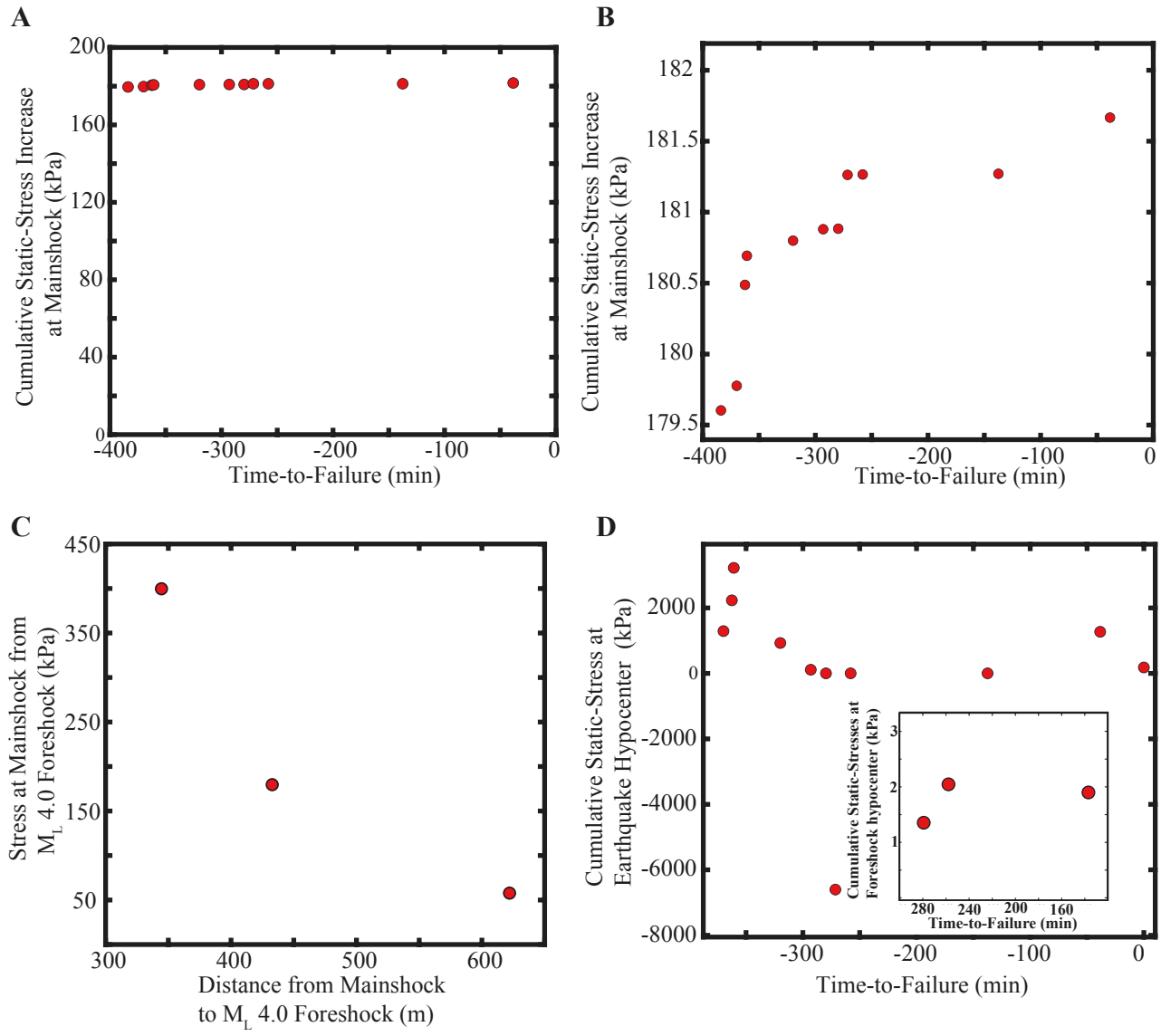

Figure 5 A: Cumulative static-stress increase at the hypocenter of the Mentone mainshock. Static-stresses associated with the initial M_L 4.0 foreshock are computed using derived source properties from EGFs. For the smaller M_L 1-2 earthquakes, we model static stresses assuming a 2 MPa stress drop. The first foreshock (M_L 4.0) imparted ~ 180 kPa of stress at the location of the Mentone mainshock. B: Zoom of data in panel A. The smaller M_L 1-2 earthquakes add < 2 kPa of stress at the hypocenter of the mainshock. C: Static stresses induced at the Mentone mainshock from the initial M_L 4.0 foreshock as a function of distance between the mainshock and foreshock. The range in distances accounts for location uncertainties in both events. The highest modeled stress occurs when the distance between the events is minimized while the lowest modeled stress occurs when the distance between events is maximized. D: Cumulative static-stresses at the hypocenter of the "current" earthquakes labeled in Figure 4. Each dot represents the total static stresses imparted from previous earthquakes. Data show that 9/11 earthquakes nucleated in areas that experienced an increase in shear stress from previous foreshocks. Only one event (TTF -271 s) nucleated in an area where the shear stress decreased. Also, note that events with TTF of 137.5, 257, and 279 (s) nucleated in areas where the shear stress increased between $1 - 2$ kPa.

initial stressing perturbations from fluid injection.

3.1 The role of the M_L 4.0 foreshock on the initiation of the Mentone M_L 4.9 mainshock

Our results indicate that the initial M_L 4.0 foreshock played a significant role in altering the stress state along the fault leading up to the 2020 M_w 4.8 Mentone mainshock (Figures 4-5, S8-S10). The M_L 4.0 foreshock nucleated ~432 m from the Mentone mainshock, and thus, static stresses from the M_L 4.0 likely played an important role in controlling the onset of the mainshock, as demonstrated in Figures 4-5. Static-stress perturbations following large earthquakes are common and elevated stresses can extend several kilometers away from the fault (King et al., 1994; Stein, 1999). Irrespective of the stress drops of the small M_L 1-2 events, our work shows that the initial M_L 4.0 foreshock imparted between ~60-400 kPa of shear stress at the hypocenter of the mainshock, clearly capable of triggering the mainshock and/or at the very least leading to a significant clock-advance in failure time. It is important to note

that the stresses decay rapidly away from the rupture tip (e.g., Figure S7B), so modest changes in event locations translate to relatively large changes in modeled stresses. The static-stresses induced at the mainshock are robust to the choice of stress drops for the small M_L 1-2 foreshocks because most of the static-stresses that are induced at the mainshock hypocenter are caused by the initial M_L 4.0 (Figure 5A; S10A). It's important to acknowledge the uncertainties in the stress drop measurements and event locations will shift the locations of the maxima and minima in the modeled stresses. In particular, the source spectral models (e.g., Brune, 1970) assume that the earthquake rupture behaves as a circular crack with constant stress drop and that the corner frequency of the source spectrum is inversely proportional to the source radius. This is a common assumption in many modeling studies, though it may oversimplify some aspects of earthquake source processes (Abercrombie, 2021; Skoumal et al., 2020; Jia et al., 2023). Nevertheless, without high-quality seismic and geodetic data it is difficult to constrain the precise details of the rupture process. Hence, the modeled stresses in Figures 4-5 should be interpreted with caution, as heterogeneity in rupture propagation will change the spatiotemporal slip and stress distribution, which in turn, will modulate the static stresses induced outside the rupture area.

The static-stresses imparted by the initial M_L 4.0 exceed the Coulomb failure stresses modeled from deep and shallow fluid injection (Tung et al., 2021; Zhai et al., 2021; Tan and Lui, 2023; Smye et al., 2024). These studies show that both deep and shallow waste-water injection increased the Coulomb failure stress at the Mentone hypocenter by 20-80 kPa through a combination of pore-pressure and poroelastic effects. These models estimate pore-pressure and poroelastic stresses using monthly injection data and do not have the resolution to decouple changes in pressures and stresses associated with M_L 4.0 foreshock from the mainshock. As a result, the initiation and role of the M_L 4.0 foreshock on subsequent seismicity, including the M_L 4.9 mainshock, has been overlooked and ignored in previous works. Our work clearly indicates that it is possible that the Mentone mainshock was in fact triggered from static-stresses induced by the M_L 4.0 foreshock as opposed to direct perturbations from fluid pressure or poroelastic stressing. However, because our analysis does not address the triggering mechanism of the initial M_L 4.0 foreshock, we cannot rule out the possibility that pore-pressure diffusion, poroelasticity, and other processes might have initiated the first M_L 4.0 foreshock. Nevertheless, shear-induced dilatancy and possible fracturing of the damage zone during the coseismic phase makes it difficult to imagine that changes in fluid pressure could trigger both the M_L 4.0 foreshock and the M_L 4.9 mainshock. That is, shear-induced dilatancy and rock fracturing should enhance the local permeability around the hypocenter, which would lead to a transient decrease in pore-pressure during/shortly after the M_L 4.0 (Sibson, 1992; Segall and Rice, 1995; Samuelson et al., 2009; Proctor et al., 2020; Aben and Brantut, 2021; Bolton et al., 2023; Affinito et al., 2024). If the local pore-pressure dropped following the initial M_L 4.0 foreshock, then it seems unlikely that it would be able to rapidly recover in < 6.5 hours to trigger the mainshock. This reinforces the idea that static stressing from the initial M_L 4.0 foreshock likely played a key role in triggering the Mentone mainshock.

It is worth pointing out that the Mentone foreshock-mainshock sequence has strong parallels with the 2011 M_w 5.7 Prague, Oklahoma foreshock-mainshock sequence (Sumy et al., 2014; Savage et al., 2017). In particular, the 2011 M_w 5.7 Prague mainshock was preceded by a M_w 5.0 foreshock less than 24 hours before the mainshock, which in turn, imparted ~ 130 kPa of stress at the hypocenter of the mainshock. The authors also propose that pore-pressure diffusion triggered the initial foreshock, which in turn, triggered the M_w 5.7 mainshock via static stresses.

3.2 Foreshocks or aftershocks?

The events that followed the initial M_L 4.0 foreshock are challenging to explain under the context of a preslip or cascade model, making it difficult to characterize these events as classic foreshocks to the impending mainshock. First, the events that follow the initial M_L 4.0 foreshock do not systematically track the static-stresses induced by previous foreshocks (Figures 4-5). In other words, each foreshock does not always nucleate and abut near the boundaries of the former foreshock as would occur in a cascading series of ruptures described under the cascade model (e.g., Yoon et al., 2019; Ellsworth and Bulut, 2018; Wu and McLaskey, 2022; Zhu et al., 2022). Rather, 6/11 events (TTF 369,362,360,319,293 min) nucleated in the surrounding rupture area of the initial 4.0 foreshock (Figures 3-4), and perhaps are better characterized as aftershocks. Also note that three events (TTF: 369, 362, and 360 mins) nucleated in areas where the shear stress increased by as much as ~ 2 MPa (Figure 5D). A total of 9/11 events nucleated in areas that experienced an increase in shear stress from the initial M_L 4.0 foreshock, albeit three of these events occurred in areas where the stress increased by only 1-3 kPa (Figure 5D).

Furthermore, the 11 events that preceded the Mentone mainshock do not exhibit features that are indicative of a preslip model. For example, in the preslip model it is thought that the nucleation zone that encompasses foreshocks expands in time and space. If foreshocks are a byproduct of a preslip model then one would expect growth in foreshock activity in space and time leading up to the mainshock (e.g., Dodge et al., 1996; Kato et al., 2016a,b). In addition, foreshocks should trend outwards and towards the mainshock hypocenter if the nucleation zone grows with time. However, the 11 earthquakes that preceded the Mentone mainshock do not exhibit such characteristics. Because repeaters represent the failure of asperities due to loading from aseismic creep, they provide additional support for a preslip model. Although 4/11 events can be characterized as repeaters (e.g., Figure 3), these events cluster around the rupture area of the initial M_L 4.0 foreshock and could also be explained by af-

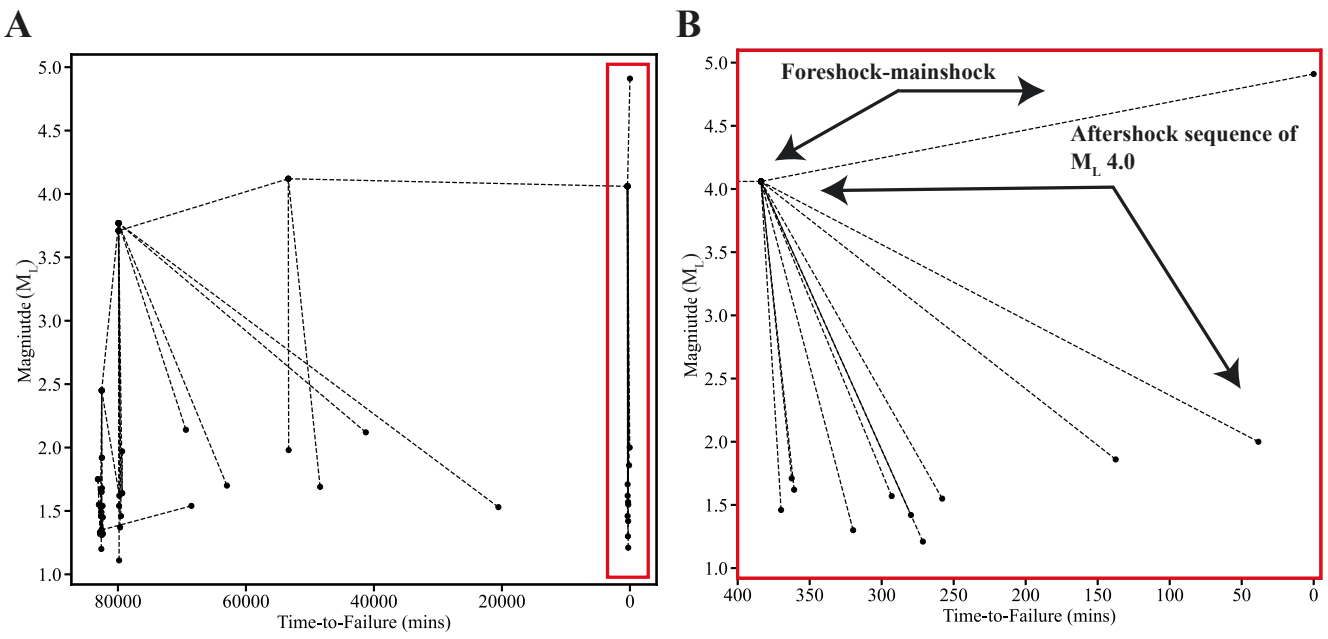

Figure 6 A: Nearest-neighbor distance linkages estimated using the distance metric defined in **?**. Black dotted lines define linkages (i.e., nearest neighbors) between pairs of earthquakes. B: Zoom of the sequence of 11 earthquakes that preceded the Mentone mainshock. The initial M_L 4.0 is linked to 10 smaller earthquakes and the Mentone mainshock. The M_L 4.0 is considered the parent of the 10 small events and the mainshock, and thus, indicates that the 10 smaller M_L 1-2 events are likely aftershocks of the M_L 4.0. In addition, the link between the M_L 4.0 and mainshock indicates that 4.0 can be considered as a foreshock to the mainshock.

terslip driven by the initial M_L 4.0 foreshock.

Based on the observations highlighted above, we propose that at least 6/11 events are in fact aftershocks of the initial M_L 4.0 as opposed to classic foreshocks of the Mentone mainshock. Specifically, events with TTF of 369, 362, 360, 319, 293, and 38 (minutes) are likely aftershocks because they cluster around the rupture area of the initial 4.0 foreshock. We test this hypothesis by following the work of **??** and measure the nearest neighbor distance (NND) for each event in our catalog using the distance metric defined in Zaliapin et al. (2008) and **?**. Specifically, the NND is obtained by minimizing the following:

$$\eta_{i,j} = \begin{cases} t_{i,j}(r_{ij}^{df})10^{-bm_i} & t_{i,j} > 0 \\ \infty & t_{i,j} \leq 0 \end{cases} \quad (5)$$

Where $t_{i,j}$ is the time between two events *i*, *j* and is positive if event *i* occurs before j; r_{ij} represents the distance between the events, *df* is the fractal dimension of event locations, *b* is the Gutenberg-Richter b-value, and m_i is the magnitude of event *i*. Here, we set *b*=1 and *df* =1.6, consistent with **?**. In short, the NND for a given event *j* is defined as the minimum distance between event *j* and all previous events in the catalog. The event *i* that represents the NND of event *j* is then said to be the parent of event *j*. In Figure 6, we plot the nearest-neighbor links for the entire catalog (e.g., Figure 1). The M_L 4.0 that occurred ~ 6.5 hours before the mainshock is linked to a previous M_L 4.0 earthquake, 10 smaller M_L 1-2 events, and the M_L 4.9 mainshock. The distance linkages in Figure 6 imply that the M_L 4.0 is the parent of the 10 smaller M_L 1-2 events and the Mentone mainshock. In other words, the 10 smaller M_L 1-2 events that followed the M_L 4.0 can be considered as aftershocks of the M_L 4.0. In addition, the linkage between the M_L 4.0 and mainshock indicates that the M_L 4.0 can be considered as a foreshock to the M_L 4.9 mainshock (**?**). In summary, the NND analysis supports the hypothesis that most of the events that followed the initial M_L 4.0 are in fact aftershocks as opposed to foreshocks of the mainshock.

We propose that aftershocks of the initial 4.0 are driven by elevated static stresses imparted by the M_L 4.0 foreshock (King et al., 1994; Stein, 1999) and postseismic afterslip (i.e., aseismic creep) (Hsu et al., 2006; Perfettini and Avouac, 2007; Ross et al., 2017). In particular, because 4/5 events abut the rupture area of the initial M_L 4.0 foreshock (see Figure 3B), have overlapping source radii, and have high waveform similarity it is possible that these events are repeaters and driven to failure by afterslip (Figure 3C). One possibility is that the initial M_L 4.0 triggered afterslip, which in turn, triggered the sequence of repeaters observed in Figure 3B. This idea is consistent with the work of Kato et al. (2016b) who showed that the 2016 M_w 7.0 Kumamoto mainshock was preceded by a large M_w 6.2 foreshock, which in turn, triggered afterslip and caused a sequence of migrating foreshocks/aftershocks towards the mainshock. Observations of repeaters during aftershock sequences have also been observed following large megathrust earthquakes (e.g., Chaves et al., 2020), and induced earthquakes in Oklahoma (Okamoto et al., 2022) and are thought to be driven by postseismic afterslip. It is also interesting to note that

the recurrence interval between the repeating earthquakes is small, ranging from 10 to 280 minutes. For the same fault patch to re-rupture, the shear stress released during the earthquake needs to recover and once again overcome the frictional strength of the fault. This implies that the stressing rate and frictional healing rate must be sufficiently high to accumulate 0.5-8 MPa of shear stress in a matter of minutes.

The remaining events with a TTF of 279, 271, 257, 137 (minutes) are not repeaters and cannot be easily explained by static stressing from the initial M_L 4.0 foreshock and/or stressing induced from the smaller M_L 1-2 earthquakes. The static stresses induced by the initial M_L 4.0 are <3 kPa and are likely too small to trigger these events (Figure 5B). The foreshock with a TTF of 271 (minutes) nucleated in area where the stress decreased. However, accounting for uncertainties in depth could push the location of this event outside rupture area of the initial M_L 4.0 foreshock where stresses were increased.

In summary, the spatiotemporal properties of the events that follow the initial M_L 4.0 foreshock are not entirely consistent with a preslip nor cascade model, which further supports the hypothesis that some of these events might be better classified as aftershocks as opposed to foreshocks. Our work further reinforces that idea that invoking a single mechanism is insufficient for explaining all the earthquakes leading up to the Mentone mainshock. Rather, a combination of mechanisms including static stressing from nearby earthquakes, fluid-induced perturbations from wastewater injection, and aseismic creep all likely played a role in triggering the sequence of 11 earthquakes that preceded the mainshock, as well as the mainshock itself (e.g., McLaskey, 2019; Cattania and Segall, 2021).

3.3 The time delay between the 4.0 foreshock and mainshock

The fact that there is a delay time of ~ 6.5 hours between the M_L 4.0 foreshock and mainshock is likely an indicator of fault zone heterogeneity, in the form of stresses or frictional strength. The delay time between these events could also indicate that the loading rate and/or mechanism that is driving failure has changed between the two events. As noted above, the static stresses from the 10 M_L 1-2 foreshocks only imparted ~1-2 kPa of stress at the hypocenter of the mainshock (Figure 5B). Though it's possible that these stresses led to the initiation of the mainshock, they likely played a minor role.

As proposed above it's possible that the initial M_L 4.0 foreshock triggered afterslip, which in turn, loaded the fault patch that hosted the mainshock. Though we lack geodetic measurements to confirm the presence of afterslip, the presence of repeaters provides some confidence in this assumption (Figure 3). If true, then perhaps the mainshock was triggered by a combination of the initial stress perturbation from the M_L 4.0 foreshock and additional loading from post-seismic afterslip of the M_L 4.0.

The delay time between the foreshock and mainshock could also be explained by a slip- and time-dependent nucleation phase of the Mentone mainshock (e.g., Dieterich, 1978, 1986). The preslip model of foreshock occurrence would support the idea of an extended nucleation phase (McLaskey, 2019). The fact that foreshocks do not exhibit spatiotemporal characteristics of a preslip model does not necessarily rule out the possibility that the mainshock was preceded by an extended nucleation phase; it simply means that foreshocks may not be a manifestation of this extended nucleation phase.

3.4 Induced Earthquakes: Fluid-induced swarms versus foreshock-mainshock-aftershock sequences

Injection induced earthquakes are often characterized as earthquake swarms as they consist of small magnitude events that lack a mainshock-aftershock sequence (e.g., Skoumal et al., 2015; Goebel et al., 2017; Skoumal and Trugman, 2021). Earthquake swarms are common features along tectonic fault zones and are thought to be triggered by natural changes in fluid pressure as opposed to far-field plate tectonic loading (e.g., Vidale and Shearer, 2006; Roland and McGuire, 2009; Goebel et al., 2017; Ross et al., 2020; Kato, 2023; Shelly, 2024; Wang et al., 2024b). Perturbations in fluid pressure are also invoked to explain moderate to large (M >= 4.0) induced earthquakes that have characteristic mainshock-aftershock sequences (Keranen et al., 2013; Sumy et al., 2014; Chen et al., 2017; Keranen and Weingarten, 2018; Skoumal et al., 2020; Tung et al., 2021; Smye et al., 2024). Hence, elevated fluid pressure alone is not indicative of whether a fault will be more prone to swarm-like behavior or mainshock-aftershock behavior and warrants the question as to what causes swarms as opposed to characteristic mainshock-aftershock sequences, such as the 2020 Mentone sequence analyzed here.

Earthquake size is a distinguishing feature that separates characteristic mainshock-aftershock sequences from earthquake swarms. It therefore follows that understanding the physical processes that control the overall event size may lend insights into the differences between swarms and mainshock-aftershock sequences. Laboratory experiments indicate that the initial stress state, relative to the shear strength, plays a key role in regulating earthquake size (e.g., Passelègue et al., 2020; Cebry et al., 2022). If the initial stress state on the fault is low relative to its shear strength, it could prevent the nucleation of a large earthquake because there is less elastic-strain energy that can be used to drive frictional slip. A low initial stress state is possible if the loading rate from external sources (e.g., far-field plate tectonic loading, aseismic creep, or fluid-induced processes) is high relative to the frictional healing rate. Rapid loading with modest and/or negligible healing would facilitate the occurrence of small earthquakes and inhibit the nucleation of large earthquakes (e.g., Shreedharan et al., 2023). In addition, a low initial stress state will require higher fluid pressure to initiate failure, which will lower the effective stress and promote small instabilities (e.g., Leeman et al., 2016). Hence, fluid-induced swarms may reflect the reactivation of faults that have a low initial stress state relative to their failure strength.

In contrast, foreshock-mainshock-aftershock sequences, such as the Mentone sequence analyzed here, might be more common in situations where the initial stress is high relative to its shear strength. If the initial stress is high, there is more elastic strain energy that can be used to drive frictional slip, resulting in larger magnitude events (e.g., Passelègue et al., 2020). In addition, less fluid pressure is needed to initiate slip, which would allow the effective normal stress to remain high and promote the occurrence of large instabilities (Leeman et al., 2016). The Mentone sequence and other moderate to large, induced earthquakes (e.g., Keranen et al., 2013; Sumy et al., 2014; Chen et al., 2017; Keranen and Weingarten, 2018; Tung et al., 2021) might be examples of such phenomena.

4 Conclusion

The 2020 M_w 4.8 Mentone earthquake was preceded by a sequence of 11 earthquakes that occurred in the final ~ 6.5 hours leading up to the mainshock. Seismicity in west Texas is thought to be largely driven by subsurface fluid injection from oil-gas operations. However, here we show that earthquake-earthquake triggering played an important role in the nucleation of the 2020 Mentone earthquake sequence. The initial M_L 4.0 foreshock significantly altered the local shear stress along the fault plane. The mainshock and most (9/11) of the earthquakes that preceded it nucleated in areas where the static shear stresses were increased from the initial 4.0 foreshock. The sequence of earthquakes that preceded the mainshock do not exhibit systematic spatiotemporal characteristics that are indicative of a preslip or cascade model, making it challenging to characterize them as classic foreshocks. Statistical attributes and source properties indicate that at least (6/11) of these earthquakes are likely aftershocks of the initial 4.0 as opposed to foreshocks to the Mentone mainshock. Our work shows that a combination of physical processes including, static stress transfer from earthquake-earthquake triggering, aseismic creep, and fluid-induced stress changes all played an important role in triggering the Mentone mainshock and the sequence of 11 earthquakes that preceded it.

5 Data and resources

The raw waveform data used in this study are provided in the following link: https://dataverse.tdl.org/dataset.xhtml?persistentId=doi:10.18738/T8/GHRTZQ. The supplement contains a set of complementary figures that clarify the methods, estimates of source properties, and additional modeling results.

6 Acknowledgements

The authors thank Texas Seismological Network seismic analysts for technical support, Lilly Horne for providing the fault plane solution, and Prof. Bill Ellsworth for providing the slip and stress analysis code. D.C.B acknowledges funding from corporate sponsors of the Center for Injection and Seismicity Research (CISR). D.T.T. gratefully acknowledges support from the National Science Foundation under award EAR-2231705. A.S. and Y.C. acknowledges support from the State of Texas, Texas Seismological Network and Seismology Research (TexNet) program.

References

Aben, F. M. and Brantut, N. Dilatancy stabilises shear failure in rock. *Earth and Planetary Science Letters*, 574:117174, 2021. doi: 10.1016/j.epsl.2021.117174.

Abercrombie, R. E. Resolution and uncertainties in estimates of earthquake stress drop and energy release. *Philosophical Transactions of the Royal Society A: Mathematical, Physical and Engineering Sciences*, 379(2196):20200131, Mar. 2021. doi: 10.1098/rsta.2020.0131.

Abercrombie, R. E. and Mori, J. Occurrence patterns of foreshocks to large earthquakes in the western United States. *Nature*, 381 (6580):303–307, May 1996. doi: 10.1038/381303a0.

Abercrombie, R. E., Agnew, D. C., and Wyatt, F. K. Testing a model of earthquake nucleation. *Bulletin of the Seismological Society of America*, 85(6):1873–1878, Dec. 1995. doi: 10.1785/bssa0850061873.

Affinito, R., Elsworth, D., Mittal, T., Scuderi, M. M., and Marone, C. Rate and Pressure Dependence of Dilatancy and Fault Strength in Partially-Drained Laboratory Fault Zones. Oct. 2024. doi: 10.22541/essoar.172798807.76814555/v1.

Andrews, D. J. A stochastic fault model: 1. Static case. *Journal of Geophysical Research: Solid Earth*, 85(B7):3867–3877, July 1980. doi: 10.1029/jb085ib07p03867.

Beroza, G. C. and Ellsworth, W. L. Properties of the seismic nucleation phase. *Tectonophysics*, 261(1–3):209–227, Aug. 1996. doi: 10.1016/0040-1951(96)00067-4.

Bolton, D., Affinito, R., Smye, K., Marone, C., and Hennings, P. Frictional and poromechanical properties of the Delaware Mountain Group: Insights into induced seismicity in the Delaware Basin. *Earth and Planetary Science Letters*, 623:118436, 2023.

Bolton, D. C., Shreedharan, S., Rivière, J., and Marone, C. Frequency-Magnitude Statistics of Laboratory Foreshocks Vary With Shear Velocity, Fault Slip Rate, and Shear Stress. *Journal of Geophysical Research: Solid Earth*, 126(11), Nov. 2021. doi: 10.1029/2021jb022175.

Bouchon, M., Karabulut, H., Aktar, M., Özalaybey, S., Schmittbuhl, J., and Bouin, M.-P. Extended Nucleation of the 1999 M w 7.6 Izmit Earthquake. *Science*, 331(6019):877–880, Feb. 2011. doi: 10.1126/science.1197341.

Bouchon, M., Durand, V., Marsan, D., Karabulut, H., and Schmittbuhl, J. The long precursory phase of most large interplate earthquakes. *Nature Geoscience*, 6(4):299–302, Mar. 2013. doi: 10.1038/ngeo1770.

Brodsky, E. E. The importance of studying small earthquakes. *Science*, 364(6442):736–737, May 2019. doi: 10.1126/science.aax2490.

Brodsky, E. E. and Lay, T. Recognizing Foreshocks from the 1 April 2014 Chile Earthquake. *Science*, 344(6185):700–702, May 2014. doi: 10.1126/science.1255202.

Brune, J. N. Tectonic stress and the spectra of seismic shear waves from earthquakes. *Journal of Geophysical Research*, 75(26): 4997–5009, Sept. 1970. doi: 10.1029/jb075i026p04997.

Cappa, F., Scuderi, M. M., Collettini, C., Guglielmi, Y., and Avouac, J.-P. Stabilization of fault slip by fluid injection in the laboratory

and in situ. *Science Advances*, 5(3), Mar. 2019. doi: 10.1126/sciadv.aau4065.

Cattania, C. and Segall, P. Precursory Slow Slip and Foreshocks on Rough Faults. *Journal of Geophysical Research: Solid Earth*, 126 (4):e2020JB020430, 2021. doi: 10.1029/2020JB020430.

Cebry, S. B., Ke, C.-Y., and McLaskey, G. The Role of Background Stress State in Fluid-Induced Aseismic Slip and Dynamic Rupture on a 3-m Laboratory Fault. *Journal of Geophysical Research: Solid Earth*, 127(8), Mar. 2022. doi: 10.1029/2022JB024371.

Cebry, S. B. L. and McLaskey, G. C. Seismic swarms produced by rapid fluid injection into a low permeability laboratory fault. *Earth and Planetary Science Letters*, 557:116726, Mar. 2021. doi: 10.1016/j.epsl.2020.116726.

Chaves, E., Schwartz, S., and Abercrombie, R. Repeating earthquakes record fault weakening and healing in areas of megathrust postseismic slip. *Science Advances*, 6(32):eaaz9317, 2020. doi: 10.1126/sciadv.aaz9317.

Chen, X. and Shearer, P. M. California foreshock sequences suggest aseismic triggering process. *Geophysical Research Letters*, 40 (11):2602–2607, June 2013. doi: 10.1002/grl.50444.

Chen, X. and Shearer, P. M. Analysis of Foreshock Sequences in California and Implications for Earthquake Triggering. *Pure and Applied Geophysics*, 173(1):133–152, May 2015. doi: 10.1007/s00024-015-1103-0.

Chen, X., Nakata, N., Pennington, C., Haffener, J., Chang, J. C., He, X., Zhan, Z., Ni, S., and Walter, J. I. The Pawnee earthquake as a result of the interplay among injection, faults and foreshocks. *Scientific Reports*, 7(1), July 2017. doi: 10.1038/s41598-017-04992-z.

Dieterich, J. Preseismic fault slip and earthquake prediction. *Journal of Geophysical Research: Solid Earth*, 83(B8):3940–3948, 1978.

Dieterich, J. A model for the nucleation of earthquake slip. *Earthquake source mechanics*, 37:37–47, 1986.

Dieterich, J. H. Earthquake nucleation on faults with rate-and state-dependent strength. *Tectonophysics*, 211(1–4):115–134, Sept. 1992. doi: 10.1016/0040-1951(92)90055-b.

Dodge, D. A., Beroza, G. C., and Ellsworth, W. L. Detailed observations of California foreshock sequences: Implications for the earthquake initiation process. *Journal of Geophysical Research: Solid Earth*, 101(B10):22371–22392, Oct. 1996. doi: 10.1029/96jb02269.

Dresen, G., Kwiatek, G., Goebel, T., and Ben-Zion, Y. Seismic and Aseismic Preparatory Processes Before Large Stick–Slip Failure. *Pure and Applied Geophysics*, 177(12):5741–5760, Oct. 2020. doi: 10.1007/s00024-020-02605-x.

Ellsworth, W. L. and Beroza, G. C. Seismic Evidence for an Earthquake Nucleation Phase. *Science*, 268(5212):851–855, May 1995. doi: 10.1126/science.268.5212.851.

Ellsworth, W. L. and Bulut, F. Nucleation of the 1999 Izmit earthquake by a triggered cascade of foreshocks. *Nature Geoscience*, 11(7):531–535, June 2018. doi: 10.1038/s41561-018-0145-1.

Eshelby, J. D. The determination of the elastic field of an ellipsoidal inclusion, and related problems. *Proceedings of the royal society of London. Series A. Mathematical and physical sciences*, 241 (1226):376–396, 1957. doi: 10.1098/rspa.1957.0133.

Geller, R. Earthquake prediction: a critical review. *Geophysical Journal International*, 131(3):425–450, 1997.

Goebel, T., Weingarten, M., Chen, X., Haffener, J., and Brodsky, E. The 2016 Mw5.1 Fairview, Oklahoma earthquakes: Evidence for long-range poroelastic triggering at gt;40 km from fluid disposal wells. *Earth and Planetary Science Letters*, 472:50–61, Aug. 2017. doi: 10.1016/j.epsl.2017.05.011.

Goebel, T. H. W. and Brodsky, E. E. The spatial footprint of injection wells in a global compilation of induced earthquake sequences. *Science*, 361(6405):899–904, Aug. 2018. doi: 10.1126/science.aat5449.

Gomberg, J. Unsettled earthquake nucleation. *Nature Geoscience*, 11(7):463–464, June 2018. doi: 10.1038/s41561-018-0149-x.

Grigoratos, I., Savvaidis, A., and Rathje, E. Distinguishing the Causal Factors of Induced Seismicity in the Delaware Basin: Hydraulic Fracturing or Wastewater Disposal? *Seismological Research Letters*, 93(5):2640–2658, June 2022. doi: 10.1785/0220210320.

Guglielmi, Y., Cappa, F., Avouac, J.-P., Henry, P., and Elsworth, D. Seismicity triggered by fluid injection–induced aseismic slip. *Science*, 348(6240):1224–1226, June 2015. doi: 10.1126/science.aab0476.

Helmstetter, A. and Sornette, D. Foreshocks explained by cascades of triggered seismicity. *Journal of Geophysical Research: Solid Earth*, 108(B10), Oct. 2003. doi: 10.1029/2003jb002409.

Horne, E. A., Hennings, P. H., and Zahm, C. K. *Basement-rooted faults of the Delaware Basin and Central Basin Platform, Permian Basin, West Texas and southeastern New Mexico*. Apr. 2021. doi: 10.23867/ri0286c6.

Hsu, Y.-J., Simons, M., Avouac, J.-P., Galetzka, J., Sieh, K., Chlieh, M., Natawidjaja, D., Prawirodirdjo, L., and Bock, Y. Frictional Afterslip Following the 2005 Nias-Simeulue Earthquake, Sumatra. *Science*, 312(5782):1921–1926, June 2006. doi: 10.1126/science.1126960.

Huang, G.-c. D., Horne, E., Kavoura, F., and Savvaidis, A. Characteristics of Seismogenic Structures and 3D Stress State of the Delaware Basin of West Texas as Constrained by Earthquake Source Mechanisms. *Seismological Research Letters*, 93(6): 3363–3372, Aug. 2022. doi: 10.1785/0220220054.

Jia, Z., Jin, Z., Marchandon, M., Ulrich, T., Gabriel, A.-A., Fan, W., Shearer, P., Zou, X., Rekoske, J., Bulut, F., Garagon, A., and Fialko, Y. The complex dynamics of the 2023 Kahramanmaraş, Turkey,Mw7.8-7.7 earthquake doublet. *Science*, 381 (6661):985–990, Sept. 2023. doi: 10.1126/science.adi0685.

Jin, L., Curry, W. J., Lippoldt, R. C., Hussenoeder, S. A., and Bhargava, P. 3D coupled hydro-mechanical modeling of multi-decadal multi-zone saltwater disposal in layered and faulted poroelastic rocks and implications for seismicity: An example from the Midland Basin. *Tectonophysics*, 863:229996, Sept. 2023. doi: 10.1016/j.tecto.2023.229996.

Jones, L. and Molnar, P. Frequency of foreshocks. *Nature*, 262 (5570):677–679, Aug. 1976. doi: 10.1038/262677a0.

Kato, A. Implications of Fault-Valve Behavior From Immediate Aftershocks Following the 2023 Mj6.5 Earthquake Beneath the Noto Peninsula, Central Japan. *Geophysical Research Letters*, 51(1), Dec. 2023. doi: 10.1029/2023gl106444.

Kato, A., Obara, K., Igarashi, T., Tsuruoka, H., Nakagawa, S., and Hirata, N. Propagation of Slow Slip Leading Up to the 2011 M w 9.0 Tohoku-Oki Earthquake. *Science*, 335(6069):705–708, Feb. 2012. doi: 10.1126/science.1215141.

Kato, A., Fukuda, J., Kumazawa, T., and Nakagawa, S. Accelerated nucleation of the 2014 Iquique, Chile Mw 8.2 Earthquake. *Scientific Reports*, 6(1), Apr. 2016a. doi: 10.1038/srep24792.

Kato, A., Fukuda, J., Nakagawa, S., and Obara, K. Foreshock migration preceding the 2016 Mw 7.0 Kumamoto earthquake, Japan. *Geophysical Research Letters*, 43(17):8945–8953, Sept. 2016b. doi: 10.1002/2016gl070079.

Keranen, K. M. and Weingarten, M. Induced Seismicity. *Annual Review of Earth and Planetary Sciences*, 46(1):149–174, May 2018. doi: 10.1146/annurev-earth-082517-010054.

Keranen, K. M., Savage, H. M., Abers, G. A., and Cochran, E. S. Potentially induced earthquakes in Oklahoma, USA: Links between wastewater injection and the 2011 Mw 5.7 earthquake sequence. *Geology*, 41(6):699–702, June 2013. doi: 10.1130/g34045.1.

King, G. C., Stein, R. S., and Lin, J. Static stress changes and the triggering of earthquakes. *Bulletin of the Seismological Society of America*, 84(3):935–953, 1994. doi: 10.1785/BSSA0840030935.

Kwiatek, G., Martínez-Garzón, P., Becker, D., Dresen, G., Cotton, F., Beroza, G. C., Acarel, D., Ergintav, S., and Bohnhoff, M. Months-long seismicity transients preceding the 2023 MW 7.8 Kahramanmaraş earthquake, Türkiye. *Nature Communications*, 14(1), Nov. 2023. doi: 10.1038/s41467-023-42419-8.

Leeman, J. R., Saffer, D. M., Scuderi, M. M., and Marone, C. Laboratory observations of slow earthquakes and the spectrum of tectonic fault slip modes. *Nature Communications*, 7(1), Mar. 2016. doi: 10.1038/ncomms11104.

Martínez-Garzón, P. and Poli, P. Cascade and pre-slip models oversimplify the complexity of earthquake preparation in nature. *Communications Earth & Environment*, 5(1), Mar. 2024. doi: 10.1038/s43247-024-01285-y.

McLaskey, G. C. Earthquake Initiation From Laboratory Observations and Implications for Foreshocks. *Journal of Geophysical Research: Solid Earth*, 124(12):12882–12904, Dec. 2019. doi: 10.1029/2019jb018363.

Mignan, A. The debate on the prognostic value of earthquake foreshocks: A meta-analysis. *Scientific Reports*, 4(1), Feb. 2014. doi: 10.1038/srep04099.

Moutote, L., Itoh, Y., Lengliné, O., Duputel, Z., and Socquet, A. Evidence of a Transient Aseismic Slip Driving the 2017 Valparaiso Earthquake Sequence, From Foreshocks to Aftershocks. *Journal of Geophysical Research: Solid Earth*, 128(9), Sept. 2023. doi: 10.1029/2023jb026603.

Ohnaka, M. Earthquake source nucleation: A physical model for short-term precursors. *Tectonophysics*, 211(1–4):149–178, Sept. 1992. doi: 10.1016/0040-1951(92)90057-d.

Ohnaka, M. Critical Size of the Nucleation Zone of Earthquake Rupture Inferred from Immediate Foreshock Activity. *Journal of Physics of the Earth*, 41(1):45–56, 1993. doi: 10.4294/jpe1952.41.45.

Ohnaka, M. and Shen, L. Scaling of the shear rupture process from nucleation to dynamic propagation: Implications of geometric irregularity of the rupturing surfaces. *Journal of Geophysical Research: Solid Earth*, 104(B1):817–844, Jan. 1999. doi: 10.1029/1998jb900007.

Okamoto, K. K., Savage, H. M., Cochran, E. S., and Keranen, K. M. Stress Heterogeneity as a Driver of Aseismic Slip During the 2011 Prague, Oklahoma Aftershock Sequence. *Journal of Geophysical Research: Solid Earth*, 127(8), Aug. 2022. doi: 10.1029/2022jb024431.

Passelègue, F. X., Almakari, M., Dublanchet, P., Barras, F., Fortin, J., and Violay, M. Initial effective stress controls the nature of earthquakes. *Nature Communications*, 11(1), Oct. 2020. doi: 10.1038/s41467-020-18937-0.

Peng, H. and Mori, J. Characteristics of the foreshock occurrence for Mj3.0 to 7.2 shallow onshore earthquakes in Japan. *Earth, Planets and Space*, 74(1), Mar. 2022. doi: 10.1186/s40623-021-01567-1.

Pepin, K. S., Ellsworth, W. L., Sheng, Y., and Zebker, H. A. Shallow Aseismic Slip in the Delaware Basin Determined by Sentinel-1 InSAR. *Journal of Geophysical Research: Solid Earth*, 127(2), Oct. 2022. doi: 10.1029/2021JB023157.

Perfettini, H. and Avouac, J. Modeling afterslip and aftershocks following the 1992 Landers earthquake. *Journal of Geophysical Research: Solid Earth*, 112(B7), July 2007. doi: 10.1029/2006jb004399.

Proctor, B., Lockner, D. A., Kilgore, B. D., Mitchell, T. M., and Beeler, N. M. Direct Evidence for Fluid Pressure, Dilatancy, and Compaction Affecting Slip in Isolated Faults. *Geophysical Research Letters*, 47(16), Aug. 2020. doi: 10.1029/2019gl086767.

Roland, E. and McGuire, J. J. Earthquake swarms on transform faults. *Geophysical Journal International*, 178(3):1677–1690, Sept. 2009. doi: 10.1111/j.1365-246x.2009.04214.x.

Ross, Z. E., Rollins, C., Cochran, E. S., Hauksson, E., Avouac, J., and Ben-Zion, Y. Aftershocks driven by afterslip and fluid pressure sweeping through a fault-fracture mesh. *Geophysical Research Letters*, 44(16):8260–8267, Aug. 2017. doi: 10.1002/2017gl074634.

Ross, Z. E., Trugman, D. T., Hauksson, E., and Shearer, P. M. Searching for hidden earthquakes in Southern California. *Science*, 364 (6442):767–771, May 2019. doi: 10.1126/science.aaw6888.

Ross, Z. E., Cochran, E. S., Trugman, D. T., and Smith, J. D. 3D fault architecture controls the dynamism of earthquake swarms. *Science*, 368(6497):1357–1361, June 2020. doi: 10.1126/science.abb0779.

Ruiz, S., Metois, M., Fuenzalida, A., Ruiz, J., Leyton, F., Grandin, R., Vigny, C., Madariaga, R., and Campos, J. Intense foreshocks and a slow slip event preceded the 2014 Iquique M w 8.1 earthquake. *Science*, 345(6201):1165–1169, Sept. 2014. doi: 10.1126/science.1256074.

Saad, O. M., Chen, Y., Siervo, D., Zhang, F., Savvaidis, A., Huang, G.-c. D., Igonin, N., Fomel, S., and Chen, Y. EQCCT: A Production-Ready Earthquake Detection and Phase-Picking Method Using the Compact Convolutional Transformer. *IEEE Transactions on Geoscience and Remote Sensing*, 61:1–15, 2023. doi: 10.1109/tgrs.2023.3319440.

Samuelson, J., Elsworth, D., and Marone, C. Shear-induced dilatancy of fluid-saturated faults: Experiment and theory. *Journal of Geophysical Research: Solid Earth*, 114(B12), Dec. 2009. doi: 10.1029/2008jb006273.

Savage, H. M., Keranen, K. M., P. Schaff, D., and Dieck, C. Possible precursory signals in damage zone foreshocks. *Geophysical Research Letters*, 44(11):5411–5417, June 2017. doi: 10.1002/2017gl073226.

Savvaidis, A., Lomax, A., and Breton, C. Induced Seismicity in the Delaware Basin, West Texas, is Caused by Hydraulic Fracturing and Wastewater Disposal. *Bulletin of the Seismological Society of America*, 110(5):2225–2241, Aug. 2020. doi: 10.1785/0120200087.

Scholz, C., Molnar, P., and Johnson, T. Detailed studies of frictional sliding of granite and implications for the earthquake mechanism. *Journal of Geophysical Research*, 77(32):6392–6406, Nov. 1972. doi: 10.1029/jb077i032p06392.

Segall, P. and Lu, S. Injection-induced seismicity: Poroelastic and earthquake nucleation effects. *Journal of Geophysical Research: Solid Earth*, 120(7):5082–5103, July 2015. doi: 10.1002/2015jb012060.

Segall, P. and Rice, J. R. Dilatancy, compaction, and slip instability of a fluid-infiltrated fault. *Journal of Geophysical Research: Solid Earth*, 100(B11):22155–22171, Nov. 1995. doi: 10.1029/95jb02403.

Shelly, D. R. Examining the Connections Between Earthquake Swarms, Crustal Fluids, and Large Earthquakes in the Context of the 2020–2024 Noto Peninsula, Japan, Earthquake Sequence. *Geophysical Research Letters*, 51(4), Feb. 2024. doi: 10.1029/2023gl107897.

Shreedharan, S., Saffer, D., Wallace, L. M., and Williams, C. Ultralow frictional healing explains recurring slow slip events. *Science*, 379(6633):712–717, Feb. 2023. doi: 10.1126/science.adf4930.

Sibson, R. Implications of fault-valve behaviour for rupture nucleation and recurrence. *Tectonophysics*, 211(1–4):283–293, Sept. 1992. doi: 10.1016/0040-1951(92)90065-e.

Skoumal, R. J. and Trugman, D. T. The Proliferation of Induced Seismicity in the Permian Basin, Texas. *Journal of Geophysical Research: Solid Earth*, 126(6), June 2021. doi: 10.1029/2021jb021921.

Skoumal, R. J., Brudzinski, M. R., and Currie, B. S. Distinguishing induced seismicity from natural seismicity in Ohio: Demonstrating the utility of waveform template matching. *Journal of Geophysical Research: Solid Earth*, 120(9):6284–6296, Sept. 2015. doi: 10.1002/2015jb012265.

Skoumal, R. J., Kaven, J. O., Barbour, A. J., Wicks, C., Brudzinski, M. R., Cochran, E. S., and Rubinstein, J. L. The Induced Mw 5.0 March 2020 West Texas Seismic Sequence. *Journal of Geophysical Research: Solid Earth*, 126(1), Dec. 2020. doi: 10.1029/2020jb020693.

Smye, K., Ge, J., Morris, A., Horne, E., Calle, A., Eastwood, R., Nicot, J.-P., and Hennings, P. in review, Role of Deep Fluid Injection in Induced Seismicity in the Delaware Basin, West Texas and Southeast New Mexico. *G-Cubed*, page –, 2024.

Stein, R. S. The role of stress transfer in earthquake occurrence. *Nature*, 402(6762):605–609, 1999. doi: 10.1038/45144.

Sumy, D. F., Cochran, E. S., Keranen, K. M., Wei, M., and Abers, G. A. Observations of static Coulomb stress triggering of the November 2011 M5. 7 Oklahoma earthquake sequence. *Journal of Geophysical Research: Solid Earth*, 119(3):1904–1923, Mar. 2014. doi: 10.1002/2013jb010612.

Tan, X. and Lui, S. K. Y. Potential Poroelastic Triggering of the 2020 M5.0 Mentone Earthquake in the Delaware Basin, Texas, by Shallow Injection Wells. *Bulletin of the Seismological Society of America*, 114(2):882–894, 2023. doi: 10.1785/0120230142.

Tape, C., Holtkamp, S., Silwal, V., Hawthorne, J., Kaneko, Y., Ampuero, J. P., Ji, C., Ruppert, N., Smith, K., and West, M. E. Earthquake nucleation and fault slip complexity in the lower crust of central Alaska. *Nature Geoscience*, 11(7):536–541, June 2018. doi: 10.1038/s41561-018-0144-2.

Trugman, D. and Ross, Z. Pervasive foreshock activity across southern California. *Geophysical Research Letters*, 46(15): 8772–8781, 2019. doi: 10.1029/2019GL083725.

Trugman, D. T. and Savvaidis, A. Source Spectral Properties of Earthquakes in the Delaware Basin of West Texas. *Seismological Research Letters*, 92(4):2477–2489, Mar. 2021. doi: 10.1785/0220200461.

Trugman, D. T. and Shearer, P. M. GrowClust: A Hierarchical Clustering Algorithm for Relative Earthquake Relocation, with Application to the Spanish Springs and Sheldon, Nevada, Earthquake Sequences. *Seismological Research Letters*, 88(2A):379–391, Feb. 2017. doi: 10.1785/0220160188.

Trugman, D. T., McBrearty, I. W., Bolton, D. C., Guyer, R. A., Marone, C., and Johnson, P. A. The Spatiotemporal Evolution of Granular Microslip Precursors to Laboratory Earthquakes. *Geophysical Research Letters*, 47(16), Aug. 2020. doi: 10.1029/2020gl088404.

Tung, S., Zhai, G., and Shirzaei, M. Potential Link Between 2020 Mentone, West Texas M5 Earthquake and Nearby Wastewater Injection: Implications for Aquifer Mechanical Properties. *Geophysical Research Letters*, 48(3), Feb. 2021. doi: 10.1029/2020gl090551.

Uchida, N. and Bürgmann, R. Repeating Earthquakes. *Annual Review of Earth and Planetary Sciences*, 47(1):305–332, May 2019. doi: 10.1146/annurev-earth-053018-060119.

Vidale, J. E. and Shearer, P. M. A survey of 71 earthquake bursts across southern California: Exploring the role of pore fluid pressure fluctuations and aseismic slip as drivers. *Journal of Geophysical Research: Solid Earth*, 111(B5), May 2006. doi: 10.1029/2005jb004034.

Wang, K., Peng, Z., Liang, S., Luo, J., Zhang, K., and He, C. Migrating Foreshocks Driven by a Slow Slip Event Before the 2021 MW 6.1 Yangbi, China Earthquake. *Journal of Geophysical Research: Solid Earth*, 129(1), Jan. 2024a. doi: 10.1029/2023jb027209.

Wang, Q.-Y., Cui, X., Frank, W. B., Lu, Y., Hirose, T., and Obara, K. Untangling the environmental and tectonic drivers of the Noto earthquake swarm in Japan. *Science Advances*, 10(19), May 2024b. doi: 10.1126/sciadv.ado1469.

Wetzler, N., Brodsky, E. E., Chaves, E. J., Goebel, T., and Lay, T. Regional Characteristics of Observable Foreshocks. *Seismological Research Letters*, 94(1):428–442, Oct. 2022. doi: 10.1785/0220220122.

Wu, B. S. and McLaskey, G. C. Testing Earthquake Nucleation Length Scale with Pawnee Aftershocks. *Seismological Research Letters*, 93(4):2147–2160, Apr. 2022. doi: 10.1785/0220210184.

Yoon, C. E., Yoshimitsu, N., Ellsworth, W. L., and Beroza, G. C. Foreshocks and Mainshock Nucleation of the 1999 Mw 7.1 Hector Mine, California, Earthquake. *Journal of Geophysical Research: Solid Earth*, 124(2):1569–1582, Feb. 2019. doi: 10.1029/2018jb016383.

Zaccagnino, D., Vallianatos, F., Michas, G., Telesca, L., and Doglioni, C. Are Foreshocks Fore-Shocks? *Journal of Geophysical Research: Solid Earth*, 129(2), Feb. 2024. doi: 10.1029/2023jb027337.

Zaliapin, I. and Ben-Zion, Y. Earthquake clusters in southern California I: Identification and stability. *Journal of Geophysical Research: Solid Earth*, 118(6):2847–2864, June 2013a. doi: 10.1002/jgrb.50179.

Zaliapin, I. and Ben-Zion, Y. Earthquake clusters in southern California II: Classification and relation to physical properties of the crust. *Journal of Geophysical Research: Solid Earth*, 118(6): 2865–2877, June 2013b. doi: 10.1002/jgrb.50178.

Zaliapin, I., Gabrielov, A., Keilis-Borok, V., and Wong, H. Clustering Analysis of Seismicity and Aftershock Identification. *Physical Review Letters*, 101(1), June 2008. doi: 10.1103/physrevlett.101.018501.

Zhai, G., Shirzaei, M., and Manga, M. Widespread deep seismicity in the Delaware Basin, Texas, is mainly driven by shallow wastewater injection. *Proceedings of the National Academy of Sciences*, 118(20), May 2021. doi: 10.1073/pnas.2102338118.

Zhou, Y., Ren, C., Ghosh, A., Meng, H., Fang, L., Yue, H., Zhou, S., and Su, Y. Seismological Characterization of the 2021 Yangbi Foreshock-Mainshock Sequence, Yunnan, China: More than a Triggered Cascade. *Journal of Geophysical Research: Solid Earth*, 127(8), Apr. 2022. doi: https://doi.org/10.1029/2022JB024534.

Zhu, G., Yang, H., Tan, Y. J., Jin, M., Li, X., and Yang, W. The Cascading Foreshock Sequence of the Ms 6.4 Yangbi Earthquake in Yunnan, China. *Earth and Planetary Science Letters*, 591:117594, 2022. doi: https://doi.org/10.1016/j.epsl.2022.117594.